Identifying the pattern of breakdown in a laminar-turbulent transition via binary sequence statistics and cellular-automaton simulations

Wen Zhang,[1] Peiqing Liu,[2,3] Hao Guo,[2,3] Minping Wan,[1,*] Jianchun Wang,[1] and Shiyi Chen[1,4,†]

[1]*Department of Mechanics and Aerospace Engineering, Southern University of Science and Technology, Shenzhen, Guangdong 518055, People's Republic of China*

[2]*Key Laboratory of Aero-Acoustics (Beihang University), Ministry of Industry and Information Technology, Beijing 100191, People's Republic of China*

[3]*Key Laboratory of Fluid Mechanics (Beihang University), Ministry of Education, Beijing 100191, People's Republic of China*

[4]*State Key Laboratory of Turbulence and Complex Systems,Center for Applied Physics and Technology, College of Engineering, Peking University, Beijing 100871, People's Republic of China*

(Received 3 April 2019; published 20 August 2019)

The laminar-turbulent transition induced by two-dimensional steplike roughness is investigated focusing on the pattern of breakdown. The statistics of the turbulent burst rate is found to be significantly different from the prediction of the classical theory. A systematic investigation of the pattern of breakdown is motivated by this phenomenon. It is identified with heuristic analysis that a pattern of distributed breakdown is responsible for the deviation, in contrast to the concentrated breakdown hypothesis in the classical theory. The pattern indicates that the steps probably induced a bypass transition in present experimental setup, which is different from the current understanding about the step-induced transition. Cellular-automaton simulations are carried out to validate the heuristic analysis. The influences of quasiconcentration and non-Poisson process in spot generation on the breakdown statistics are also discussed based on the simulation results.

DOI: 10.1103/PhysRevE.100.023110

I. INTRODUCTION

As the fluid flows over a surface, a boundary layer is formed due to the viscosity of the fluid. The boundary layer will be either laminar or turbulent depending on the flow environment (e.g., the Reynolds number, the surface roughness, and the free-stream turbulence). Under proper conditions, the boundary-layer transition from laminar to turbulent occurs with significant changes in flow properties. Generally, a complete transition process consists of three stages. First, the disturbances (instability waves) are generated inside the laminar boundary layer through the receptivity mechanism [1]. Then, the disturbances grow via the modal [2] or the nonmodal approach [3] due to the instability of the boundary layer. Finally, the nonlinear growth of the disturbance leads to the generation of the three-dimensional flow structure which quickly evolves into a small patch of turbulence now known as the turbulent spot [4]. The turbulent spots grow and merge into the fully turbulent boundary layer. The process of spot generation, growth, and merger is also referred as the breakdown of the laminar flow. Although the specific physical mechanisms are different, the three stages of transition are closely related. The laminar-turbulent transition is an intriguing problem in fluid dynamics, and it is also very important in aerospace engineering due to its significant influence on skin friction and heat transfer.

Recently, there is a growing interest in the transition of the boundary layer distorted by the surface roughness. The low-profile step is one of the representative two-dimensional roughness, which leads to the flow separation at the sharp edge [5–7]. If the flow remains laminar, its original state would be gradually recovered far downstream the step [7,8]. Generally, the interaction between instability modes and the distorted base flow would give rise to a destabilizing effect on the boundary layer [5,6,8]. Edelmann and Rist [6] used an additional amplification factor for the Tollmien-Schlichting (TS) wave to characterize the step influence on the stability of the boundary layer, and this idea can be used to improve the e^N method for the transition prediction [9].

The understanding of the influences of steps is still far from complete. Worner, Rist, and Wagner [10] first noticed that the forward-facing step tends to stabilize the TS waves, and they attributed this effect to the thinner boundary layer developing on the step. The theoretical work of Wu and Hogg [11] indicates that the rapid distortion caused by the localized roughness will result in acoustic radiation of the instability wave, and they proposed a transmission coefficient to characterize the change in the energetics of the TS wave. The numerical studies of Xu *et al.* [12] confirmed the local stabilizing effect of the localized isolated roughness, but they also concluded that the overall effect is destabilizing. Xu, Lombard, and Sherwin [13] found that the effect of a smooth step depends on the step height. They showed that the destabilized effect would dominate when the step height is more than 20% of the local boundary-layer thickness, but the steps with smaller heights (5% and 12% of the local boundary-layer

*wanmp@sustech.edu.cn
†chensy@sustech.edu.cn

thickness) can effectively delay the H-type transition and even completely suppress the K-type transition.

Most existing studies on the step-induced transition are numerical and limited to the growth of the instability waves. The detailed experimental results have rarely been reported so far. From an experimental point of view, the measurement to capture the growth of the disturbance around the step is much more difficult than that in a typical boundary layer because of the flow separation and the small step height. Alternatively, the pattern of breakdown (see in Sec. II) is useful and important to reveal the transition mechanism [14,15]. Nevertheless, the investigation about the breakdown statistics has received much less attention, and almost nothing is known about the breakdown region in a step-induced transition.

In this paper, we present the detailed analysis of the pattern of the breakdown in a step-induced transition process based on experimental data. We demonstrate that the breakdown is significantly different from the assumptions of the current literatures [14,16]. In addition, numerical simulations for the breakdown processes of various patterns are carried out using a cellular-automaton model [14]. It has been shown that the simulation with a simplified model can provide macroscopic statistics of the transition process in convincing agreement with data obtained from experiments or high-resolution numerical simulations [17–21]. The cellular-automaton simulation is shown to be an efficient tool to investigate the breakdown of laminar flow since their computational costs are very low.

The remainder of the paper is organized as follows. In Sec. II, the different patterns of breakdown are briefly introduced. In Secs. III and IV, the details of the wind-tunnel experiments and the cellular-automaton simulations are introduced. In Sec. V, the experimental results are presented in comparison with existing theories. In Sec. VI, the breakdown process is analyzed from a probabilistic view to identify the pattern of breakdown. In Sec. VII, the cellular-automaton simulation results are presented to validate the heuristic analysis. In Sec. VIII, two special breakdown scenarios are discussed. In Sec. IX, a summary and conclusion of our study is provided.

II. PATTERN OF BREAKDOWN

Generally, the pattern of breakdown is about the statistical characteristics of the formation of the turbulent spots. Once a turbulent spot is generated in the boundary layer, it would move downstream at a constant velocity and its streamwise and spanwise size would grow at a constant rate [16,22,23]. The self-similar evolution of a spot is shown in Fig. 1(a). The longer time the spot exists, the larger size it would become.

The intermittency factor (γ) is one of the key parameters to characterize the transition, and it is defined as the probability to be turbulent at a streamwise position. The classical theory of breakdown (see the review of Narasimha [16]) aimed at finding a universal model to reproduce the experimental results of the growth curve of γ in the breakdown region. Emmons [4] proposed a theory that the distribution of γ can be derived from the spot generation rate, which is defined as the number of turbulent spots generated per unit space and per unit time. It was found that the prediction of γ

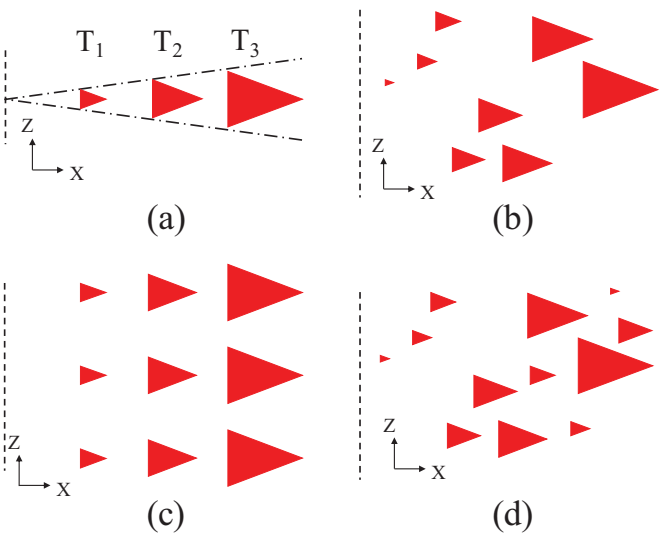

FIG. 1. Sketch of the patterns of breakdown (the red triangular areas represent the turbulent spots which are moving from the left side to the right side, the dashed line is the transition starting location, the coordinates x and z represent the streamwise and spanwise directions): (a) self-similar evolution of a single spot at different moments $T_1 < T_2 < T_3$, the dashed-dotted lines are the envelopes of the spot; (b) concentrated breakdown; (c) regular breakdown (K type); (d) distributed breakdown. (b)–(d) The snapshots of a part of the breakdown region.

can well match most of the experimental results only when the formation of spots is assumed to be concentrated at a preferred streamwise location but randomly in time and uniformly distributed in spanwise direction. This is called the hypothesis of concentrated breakdown. In a real flow, the preferred streamwise location represents a narrow band whose width is small compared to the entire breakdown region [16]. If the presence of a spot is assumed to have no effect on the generation or propagation of any other spots, then the random spot generation is a Poisson process. A snapshot of the concentrated breakdown is shown in Fig. 1(b). Note that all the spots are generated at the dashed line, and the smaller turbulent spots are always nearer to the line and the larger ones are always further downstream.

Despite some success, the classical theory based on the hypothesis of concentrated breakdown is found to be not always accurate in various transition scenarios. Johnson and Fashifar [17] noticed that their experimental data (the free-stream turbulence level Tu = 1%) cannot be well approximated by the classical theory, and they proposed a new model with a recovery period adjacent to the existing spots. Recently, Kreilos *et al.* [18] reported that the concentrated breakdown hypothesis cannot accurately reproduce their bypass transition data (Tu = 3%–4%) obtained through the direct numerical simulations.

Other examples of transitions that do not follow the classical theory are the K- and H-type transitions [24–26]. In the K- and H-type transitions, the Λ-shaped vortices are formed periodically in an aligned and staggered manner, respectively, after the exponential growth of the TS waves. Thus, the breakdown occurs in a regular pattern since the turbulent spots

are evolved from the regularly spaced Λ vortices. A sketch of the K-type regular breakdown is shown in Fig. 1(c). Note that all the spots are aligned. With this observation, Vinod and Govindarajan [14,15] argued that the spot birth might not be completely random in time and uniformly distributed in the spanwise direction. They found that the regular pattern is more likely to occur in a flow dominated by a strong instability mode like the highly decelerating flow, otherwise the breakdown is probably a mixture of the regular and the stochastic pattern. It should be noted that the theory of Vinod and Govindarajan [14,15] is still based on the assumption that the spot formation is concentrated at a preferred streamwise location.

Aside from the intermittency factor, Vinod and Govindarajan [14] proposed the other two macroscopic parameters to characterize the pattern of breakdown, i.e., the burst rate and the laminar persistence time. At a given location, the burst rate (B) is defined as the number of switchovers from laminar to turbulent flow per unit time, and the laminar persistence time (LPT) is the duration of the laminar flow between the successive switchovers. The differences between the regular breakdown and the stochastic breakdown can be observed more easily with these statistics.

As will be shown later, the present experimental results are significantly different from the prediction based on the hypothesis of concentrated breakdown, and the theory of regular breakdown does not work either. Therefore, we introduce a new pattern, the distributed breakdown, as shown in Fig. 1(d). The distributed breakdown is such a pattern that the generation of the turbulent spots is scattered in the entire breakdown region rather than a preferred streamwise location. For simplicity, we assume that the spot generation process consists of multiple Poisson processes. At each streamwise location, the random spot generation is an independent Poisson process in time and uniformly distributed in spanwise direction. As shown in Fig. 1(d), a distinct difference between the distributed and the concentrated breakdown is that the small newly generated spots can be found far downstream since these spots are not formed at the transition starting location.

III. WIND-TUNNEL EXPERIMENTS

The present experiments are performed in the closed-circuit wind tunnel at Beihang University [27]. The tunnel has a nozzle with the contraction ratio of 9:1 and a test section of 2.5 meters long with a square cross section of 1 m × 1 m. The tunnel can be operated at the inflow velocity of 0–80 m/s and the variation of the free-stream velocity is kept within ±1%. In present experiments, the inlet free-stream velocity (U_∞) is first carefully adjusted to obtain a reasonably long breakdown region, and finally fixed at about 4.5 m/s. The free-stream turbulence intensity (Tu) is less than 0.5%, which is lower than the typical level (Tu > 2%) for the bypass transition. The power spectrum of the free-stream velocity signal measured at 300 mm above the leading edge of the flat plate is shown in Fig. 2. Two peaks at 1.6 and 2.3 Hz are observed due to the low-frequency unsteadiness of the wind tunnel.

A finely polished aluminium flat plate (1 m wide) with an asymmetric leading edge is installed horizontally at the

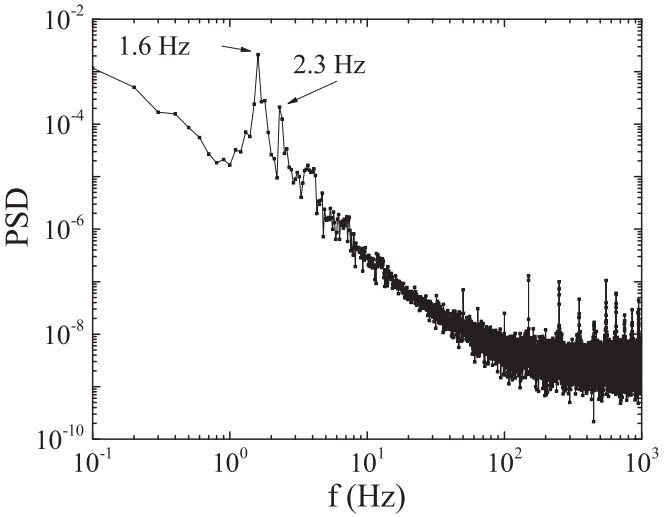

FIG. 2. Power spectrum (PSD) of the velocity signal measured in free stream at $x = 0$ mm, $y = 300$ mm.

center of the wind tunnel for the boundary-layer transition experiments. The plate is inclined to a small negative angle of attack to eliminate the potential leading-edge separation and a mild favorable pressure gradient is attained with the Falkner-Skan acceleration parameter $m = (x/U_\infty)/(dU_\infty/dx) = 0.5$ (the mean velocity profile could be found in Ref. [8]). A two-dimensional low-profile step with a rectangular cross section of 2.4 mm × 25 mm is placed on the flat plate at $x =$ 150 mm from the leading edge to trigger the laminar-turbulent transition, as shown in Fig. 3. The Reynolds number based on the step height and the free-stream velocity (Re_h) is 739, and the ratio of the step height and the local boundary-layer thickness (h/δ_{99}) is about 0.68.

The measurements are carried out at 10 equally spaced stations from $x = 550$ mm to 1000 mm in the streamwise direction to cover the breakdown region. At each station, 20–35 measurement points are scattered in the wall-normal direction throughout the boundary layer. For each point, the streamwise velocity signal is acquired with a DANTEC hot-wire anemometry system using a miniature boundary-layer

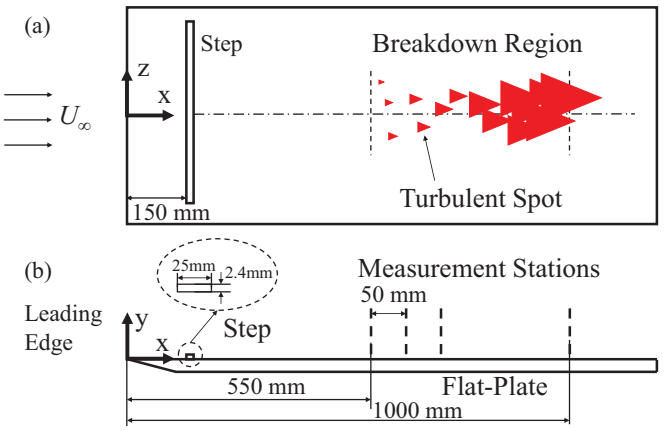

FIG. 3. Sketch of the wind-tunnel experiments of the step-induced boundary-layer transition, (a) top view, (b) side view.

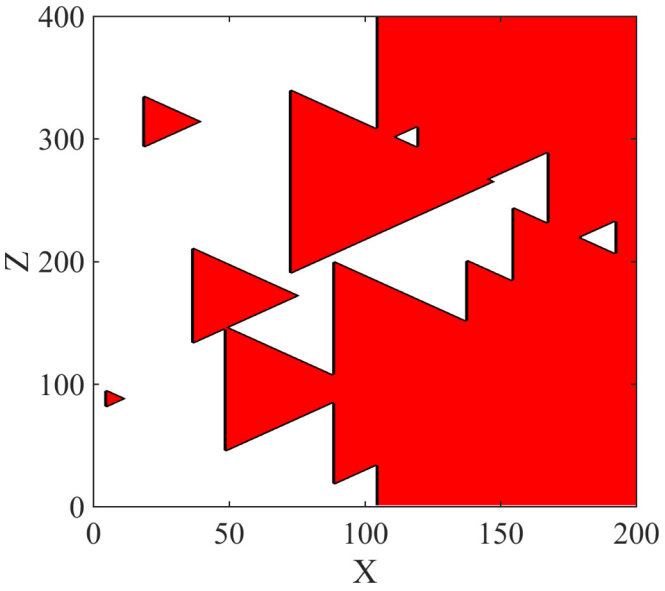

FIG. 4. A snapshot for the cellular-automaton simulation of a stochastic breakdown. The red areas represent the turbulent spots.

probe (55P15). Each hot-wire signal is digitized at a sampling rate of 10 kHz in a duration of 60 s.

IV. CELLULAR-AUTOMATON SIMULATIONS

The simulations of the laminar breakdown processes are performed using a cellular-automaton model proposed by Vinod and Govindarajan [14]. This model is based on the observation that the turbulent spots would remain self-similar and grow in a linear way as propagating toward downstream [16,22]. It has been shown that, even when the free stream is accelerated in the breakdown region (just like in present experimental setup), the spot propagation is hardly affected [23]. The two-dimensional arrowhead-shaped spots observed in previous experiments [28] are simplified to be triangular. Once generated, each spot would continuously evolve until approaching the end of the simulation region and adjacent spots would not affect each other even if the spot merger occurs. Thus, the statistical characteristics of the breakdown depends only on the pattern of spot generation.

Specifically, the breakdown is considered in a two-dimensional rectangular region which is discretized into a grid of $L_x \times L_z = 200 \times 400$ points in streamwise and spanwise directions. On each grid point, the state of the flow is assigned an integer, either 0 or 1, to represent the flow is laminar or turbulent. In each time step, the spot moves downstream for one grid location, and expands for one grid point in both the streamwise direction and two lateral sides. The different spot propagation parameter under various flow conditions [14,16] can be obtained by different aspect ratio of the grid. The periodic boundary condition is used on the two lateral sides in the spanwise direction. A snapshot of the simulation for a stochastic breakdown process is shown in Fig. 4. The turbulent spots (the red region) are evolving from left to right and finally merging into the fully turbulent region. In each simulation, the spot statistics throughout the breakdown region are obtained over 10^6 time steps to achieve statistical convergence.

The simulations are focused on various patterns of stochastic breakdown, and the parameters of the simulations are listed in Table I. For clarity, in naming the simulation cases, C is short for concentrated breakdown, D is short for distributed breakdown, and E stands for exponential distribution of the interarrival time in spot generation. The interarrival time refers to the time interval between the generation of a turbulent spot and the subsequent generation of another spot. For instance, D-E-01 refers to the first simulation case of the distributed breakdown in which the turbulent spot generation process has an exponential probability distribution of the interarrival time. A detailed introduction of the simulation setup is as follows.

The first simulation case C-E is carried out to recover the transition process described in the classical theory of concentrated breakdown and Poisson process [16], and it is also used for code validation. Specifically, in case C-E the spot generation is a single Poisson process concentrated at $X = 1$ (the upper case letters X and Z represent the discretized streamwise and spanwise locations in the simulation region). The cases D-E-01, D-E-02, and D-E-03 are simulated to validate our heuristic analysis (will be presented in Sec. V) about distributed breakdown. Particularly, a laminar-turbulent transition consisting of multiple independent spot generation processes at multiple streamwise locations would be referred as a distributed breakdown, in contrast with the concentrated breakdown of classical theory. In these simulations of distributed breakdown, at every streamwise grid location ($X = 1, 2, 3, \ldots$), a Poisson process of spot generation is simulated independently. The stochastic spot generation location is uniformly distributed in a spanwise direction in all the simulation cases.

By definition, in a Poisson process of spot generation, the number of the newly generated spots in a certain time interval is random and follows a Poisson probability distribution as

$$\Pr(k) = e^{-\lambda}\frac{\lambda^k}{k!}, \tag{1}$$

where Pr is the probability, k is the number of spots generated in a certain time interval ($k = 0, 1, 2, \ldots$), and λ is the mean and variance of spot number k. This definition is difficult to be used directly in the simulation. Equivalently, the Poisson process of spot generation can be interpreted as the interarrival time (Δt) following an exponential probability distribution as

$$\Pr(\Delta t) = \frac{1}{\beta}e^{-\Delta t/\beta}, \tag{2}$$

where β is the mean and the standard deviation of the interarrival time Δt. The average spot generation rate is inversely proportional to β, and the progress of breakdown is controlled by β in the simulations as shown in Table I. Specifically, β in case D-E-01 equals to 500 at every streamwise grid location but it is written as $\beta = 500/X^0$ to emphasize the nature of distributed breakdown. It should be noted that in the distributed breakdown, there are multiple spot generation processes, i.e., at each streamwise location, there is an independent Poisson process. Thus, we need to prescribe the parameter (β) for each Poisson process at each streamwise location. In case C-E, there is only one Poisson process and the spot generation rate is zero everywhere except the streamwise grid location $X = 1$.

TABLE I. Cellular-automaton simulation setup and parameters.

Simulation case	Interarrival time distribution	Parameter	Streamwise region of spot generation (X)	Type of breakdown
C-E	Exponential	$\beta = 15$	1	Concentrated
D-E-01	Exponential	$\beta = 500/X^0$	[1,200]	Distributed
D-E-02	Exponential	$\beta = 20000/X^1$	[1,200]	Distributed
D-E-03	Exponential	$\beta = 300000/X^{1.62}$	[1,200]	Distributed

The exponential probability distribution ($\beta = 15$) is plotted in Fig. 5 in comparison with a Poisson probability distribution ($\lambda = 15$) and a Gaussian distribution (mean $\mu = 15$ and variance $\sigma^2 = 15$). In simulations, we used discrete approximations to the exponential and Gaussian distributions. It should be noted that a Poisson distribution for the interarrival time is different from a Poisson process for the spot generation.

V. EXPERIMENTAL RESULTS

A. Turbulent spot identification

The characteristics of the velocity signals changes a lot during the transition process because of the generation and propagation of turbulent spots, as shown in Fig. 6. Near the starting position of the transition ($x = 550$ mm), only sporadic high-frequency spikelike fluctuations can be observed, which is usually interpreted as the generation of coherent vortices resulting from the nonlinear evolution of instability waves [2,29]. At down-stream stations ($x = 650$ and 750 mm), these strong coherent motions persist for longer time, and appear more frequently but still intermittently. Approaching to the end ($x = 850$ and 950 mm), the quiescent laminar flow gradually disappears until the whole signal is occupied by the strong turbulent fluctuations due to the propagation and merger of turbulent spots. As shown in Fig. 4, the spots are usually small and distant from each other in the early stage of transition, but become large enough in the late stage so that spot merger would be inevitable.

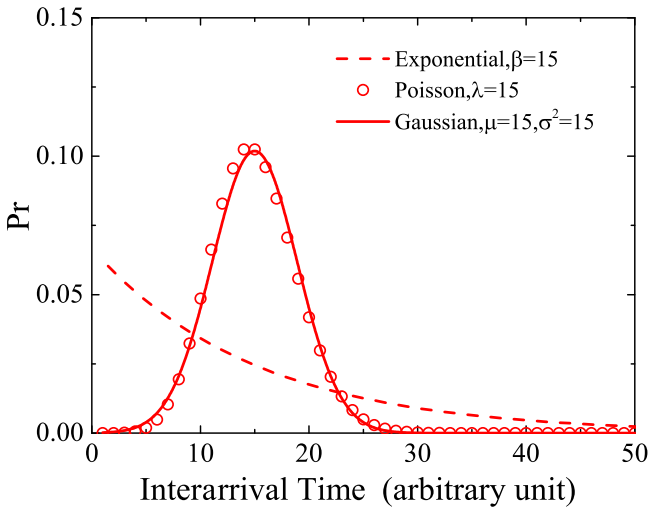

FIG. 5. Typical exponential, Poisson and Gaussian distribution for the interarrival time of turbulent spots in various patterns of breakdown.

To obtain the statistical properties of the breakdown pattern, the turbulent spots should be identified from the velocity signals first. A typical technique for turbulent spot identification is based on the instantaneous time derivatives of the velocity [30]. The accuracy of the turbulent spot identification can be evaluated from the probability distribution of the velocity derivatives [31].

The method used herein is adopted from Volino, Schultz, and Pratt [32], which has been proved to be effective and accurate for boundary-layer flows [8,32]. Generally, when the first- or second-order time derivative of the velocity is above a certain threshold, the instantaneous flow is identified as turbulent, and the intermittency function $\Gamma(t)$ is set to 1, otherwise the flow is laminar and $\Gamma(t)$ is set to 0. Finally, a binary sequence of $\Gamma(t)$ is obtained from the velocity signal

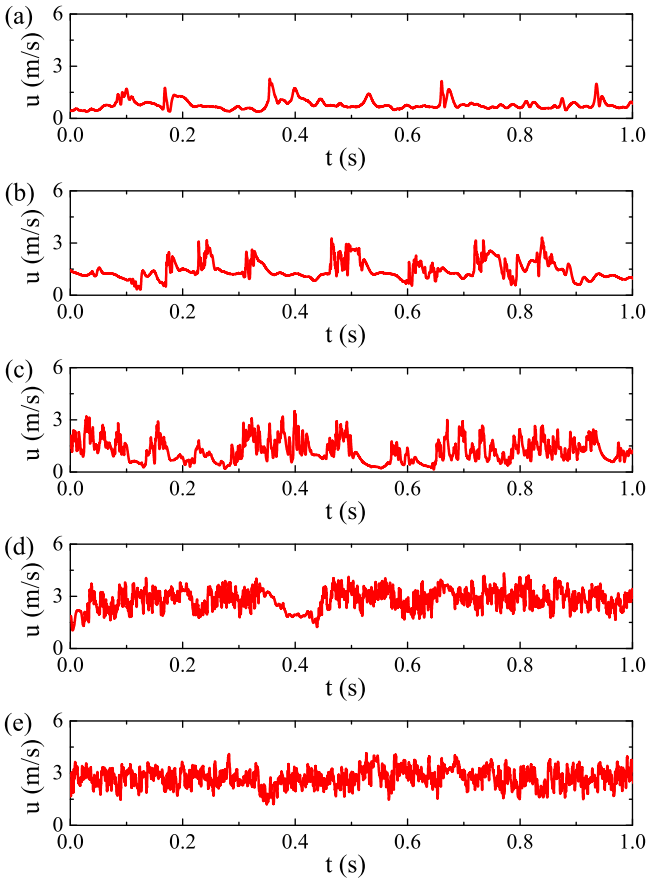

FIG. 6. Typical velocity signals throughout the transition at the same wall normal distance ($y \approx 1$ mm) and different streamwise stations (from top to bottom: $x = 550$, 650, 750, 850, and 950 mm).

which would be used in the following discussion about the pattern of breakdown.

The detailed procedure is as follows. First, the time series of velocity is high-pass filtered before the time derivatives are calculated. Generally, the high-pass filter eliminates the low-frequency fluctuations especially in the laminar flow. The large-scale structures (the low-frequency fluctuations) exist in both the laminar and turbulent flow, while the intensive small-scale coherent motions (the high-frequency fluctuations) only pertain to the turbulent flow. The high-pass filtered velocity signal $u_{\mathrm{hp}}(t)$ is obtained by

$$u_{\mathrm{hp}}(t) = \int \hat{u}(f) e^{2\pi i f t} H(f - f_{\mathrm{hp}}) df, \tag{3}$$

where f is frequency in Hz, f_{hp} is the high-pass cutoff frequency in Hz given by

$$f_{\mathrm{hp}} = C_{f_{\mathrm{hp}}} U_\infty, \tag{4}$$

where the free-stream velocity U_∞ is in m/s and the coefficient $C_{f_{\mathrm{hp}}} = 120$ (1/m). $H(f)$ is the Heaviside step function as the sharp spectral filter [33], which is defined by

$$H(f) = \begin{cases} 1, & \text{if } f \geqslant 0 \\ 0, & \text{if } f < 0 \end{cases} \tag{5}$$

$\hat{u}(f)$ is the coefficient for each Fourier mode obtained by

$$\hat{u}(f) = \int u(t) e^{-2\pi i f t} dt. \tag{6}$$

Since the filtered instantaneous velocity would cross the average line in both the laminar and turbulent zones, taking a time derivative is necessary. A first intermittency function is determined by

$$\Gamma_{1u}(t) = \begin{cases} 1, & \text{if } |\partial u_{\mathrm{hp}}/\partial t| > C_{\Gamma_{1u}} U_m U_\infty \\ 0, & \text{otherwise} \end{cases} \tag{7}$$

where the coefficient $C_{\Gamma_{1u}} = 8.89$ (1/m), and U_m is obtained with $\langle u'^2 \rangle$ and $\langle u'^3 \rangle$ (the second- and third-order central moments of the unfiltered velocity signal), by

$$U_m = \langle u \rangle + 2\langle u'^3 \rangle^{1/3} - \langle u'^2 \rangle^{1/2} \tag{8}$$

when $2\langle u'^3 \rangle^{1/3} > \langle u'^2 \rangle^{1/2}$, otherwise, $U_m = \langle u \rangle$. U_m is added to compensate the decreasing fluctuation intensity in turbulent flow close to the wall, and it is used instead of $\langle u \rangle$ in order to prevent the threshold to decrease so quickly that $\Gamma_{1u}(t)$ goes directly to 1.

Even if the high-frequency turbulent fluctuations are intensive, the first-order time derivative of the velocity might be close to 0 in the turbulent flow. Then, the second-order time derivative is also used to improve the accuracy in identifying the turbulent motions. Thus, the second intermittency function is determined by

$$\Gamma_{2u}(t) = \begin{cases} 1, & \text{if } \left|\partial^2 u_{\mathrm{hp}}/\partial t^2\right| > \text{threshold} \\ 0, & \text{otherwise.} \end{cases} \tag{9}$$

Here, the threshold is selected automatically such that

$$\langle \Gamma_{1u}(t) \rangle = \langle \Gamma_{2u}(t) \rangle. \tag{10}$$

The third intermittency function Γ_{3u} is set to 1 when either $\Gamma_{1u} = 1$ or $\Gamma_{2u} = 1$, and set to 0 when both Γ_{1u} and Γ_{2u} are 0.

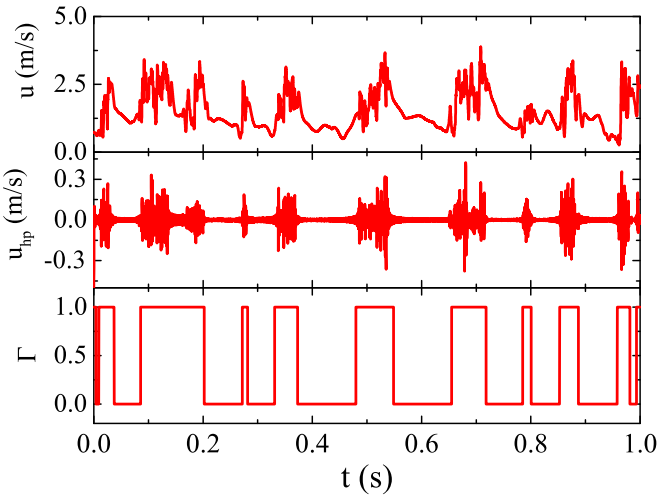

FIG. 7. Example of the laminar-turbulent separation procedure for intermittent velocity signal measured at $x = 750$ mm, $y = 1.6$ mm. From top to bottom: the original velocity signal (u), the high-pass filtered velocity signal (u_{hp}), and the binary intermittency function (Γ).

Then, to eliminate the false turbulent points in the non-turbulent flow, $\Gamma_{3u,\mathrm{lp}}$ is obtained by low-pass filtering from Γ_{3u} as

$$\Gamma_{3u,\mathrm{lp}}(t) = \int \hat{\Gamma}_{3u}(f) e^{2\pi i f t} [1 - H(f - f_{\mathrm{lp}})] df, \tag{11}$$

where f_{lp} is the low-pass cutoff frequency in Hz, and it is given by

$$f_{\mathrm{lp}} = C_{f_{\mathrm{lp}}} U_\infty, \tag{12}$$

where the coefficient $C_{f_{\mathrm{lp}}} = 17.78$ (1/m) and $\hat{\Gamma}_{3u}(f)$ is the coefficient for each Fourier mode obtained by

$$\hat{\Gamma}_{3u}(f) = \int \Gamma_{3u}(t) e^{-2\pi i f t} dt. \tag{13}$$

The final intermittency function $\Gamma(t)$ is obtained by

$$\Gamma(t) = \frac{1}{2}\left(\frac{\Gamma_{3u,\mathrm{lp}}(t) - 0.5}{|\Gamma_{3u,\mathrm{lp}}(t) - 0.5|} + 1 \right). \tag{14}$$

By definition, $\Gamma(t)$ can only be either 1 or 0 when $\Gamma_{3u,\mathrm{lp}}(t) > 0.5$ or not. All the parameters in the above procedure are suggested by Volino, Schultz, and Pratt [32], and proved to be proper for present experimental data.

The above procedure is applied to all the velocity signals measured in the breakdown region. As a typical result, the velocity signal measured at $x = 750$ mm, $y = 1.6$ mm is shown in Fig. 7 together with the corresponding high-pass filtered signal and the binary sequence of the intermittency function. The high-frequency turbulent fluctuations have been accurately identified.

B. Binary sequence statistics

As one of the key quantities in the characterization of the transition, the intermittency factor γ is defined as the probability for the flow to be turbulent at a certain location,

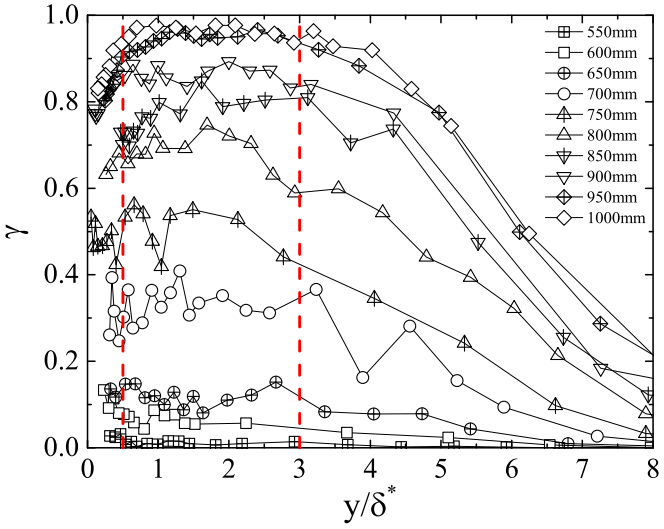

FIG. 8. Wall-normal and streamwise distributions of the experimental results of the intermittency factor (γ) in the breakdown region. The region between $y/\delta^* = 0.5$ and 3 is marked by the vertical dashed lines.

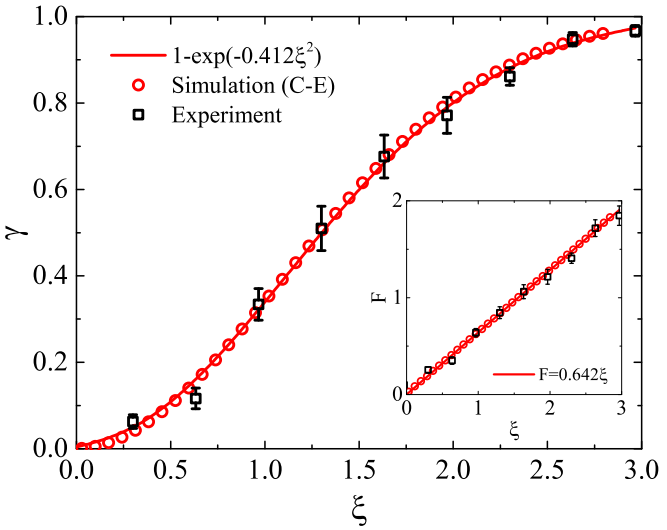

FIG. 9. Ensemble statistics of experimental results (black squares) of the intermittency factor (γ) in comparison with the prediction of classical theory (solid line) and the simulation results of case C-E (red circles) in the breakdown region. The corresponding distribution of F is shown in the inset. Error bars indicate standard deviation from the ensemble average.

and it can be estimated from the binary intermittency function by

$$\gamma = \langle \Gamma(t) \rangle. \tag{15}$$

The distribution of the experimental results of γ is shown in Fig. 8. In the streamwise direction, the maximum γ at each station increases from about 0 to approximately 1 as the flow develops from $x = 550$ mm to 1000 mm, which indicates the flow is gradually turning from laminar to turbulent. In the wall-normal direction, γ close to the wall is basically unchanged, but drops quickly at the outer edge of the boundary layer due to the interface of the near-wall turbulence and the laminar free stream. At the location very close to the wall, the intermittency statistics is affected by the rapidly decreasing mean velocity [32]. Theoretically, the intermittency factor should be the same inside the boundary layer, so the ensemble statistics is considered with the results between $y/\delta^* = 0.5$ and 3 ($\delta^* = \sqrt{\nu x/U_\infty}$ is the characteristic length scale for laminar boundary layer, where ν is the kinetic viscosity of air).

In the classical theory, the growth curve of the intermittency factor is believed to have a universal form [16], i.e.,

$$\gamma = 1 - \exp(-0.412\xi^2), \tag{16}$$

where ξ is the normalized streamwise location defined by

$$\xi = (x - x_s)/(x_{0.75} - x_{0.25}), \tag{17}$$

where x_s is the nominal starting position of the transition ($x > x_s$), $x_{0.75}$ and $x_{0.25}$ are the location where $\gamma = 0.75$ and 0.25.

The ensemble-averaged experimental results of the intermittency factor are fitted with this universal distribution, and shown in Fig. 9. The fitting result is generally good. Similar process is applied to the simulation result of the stochastic concentrated breakdown (case C-E). As shown in Fig. 9, excellent agreement between the simulation results and the universal distribution is observed. It should be noted that, unlike the simulation results, x_s and $x_{0.75} - x_{0.25}$ cannot be accurately obtained from the experimental data.

The distribution of γ can be further examined by the parameter F [14,16] defined as

$$F = \sqrt{-\ln(1-\gamma)}. \tag{18}$$

If the data follow the universal intermittency distribution, then F would be a linear function of ξ. Vinod and Govindarajan [14,15] argued that the spot merger in the late stage of transition would lead to nonlinear growth of F due to the additional regular pattern of spot generation. The regular pattern refers to the orderly arranged turbulent spots which are generated periodically, just like those in K- or H-type transition simulated by Sayadi, Hamman, and Moin [34].

$F = 0.642\xi$ is obtained directly from the universal distribution in classical theory [i.e., Eq. (16)], and as shown in the inset of Fig. 9, the experimental result of F is generally close to this straight line. As for the simulation result of case C-E, excellent agreement with the classical theory is obtained again.

Here, it should be mentioned that since F is derived from γ, then the uncertainty of F can be estimated by

$$\delta F = \frac{dF}{d\gamma}\delta\gamma, \tag{19}$$

where

$$\frac{dF}{d\gamma} = \frac{1}{2F}\frac{1}{1-\gamma}. \tag{20}$$

As γ approaches 1, $dF/d\gamma \to \infty$, so that the uncertainty of F would increase quickly when the transition is close to the end, which is consistent with the increasing error bars of F in the inset of Fig. 9. It means that the ensemble average of F observed from experimental data should be used more carefully.

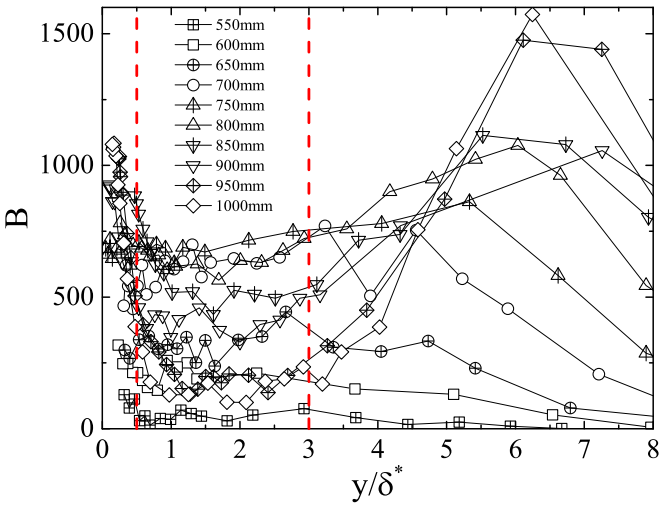

FIG. 10. Wall-normal and streamwise distributions of the experimental results of the burst rate (B) in the breakdown region. The region between $y/\delta^* = 0.5$ and 3 is marked by the vertical dashed lines.

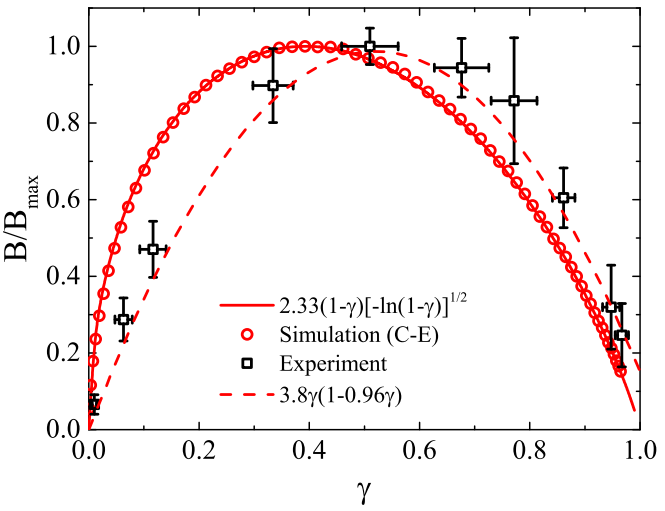

FIG. 11. Ensemble statistics of experimental results (black squares) of the normalized burst rate ($B/B_{\max}$) in comparison with the prediction of classical theory (solid line) and the simulation results of case C-E (red circles) in the breakdown region. Error bars indicate standard deviation from the ensemble average. The quadratic function (dashed line) fitted from the experimental data is also plotted.

Another easily measurable quantity in the transition process is the burst rate (B), which is estimated as the number of switchovers from 0 to 1 per unit time in the binary sequence of the intermittency function Γ. The distribution of B in the wall-normal and streamwise directions is shown in Fig. 10. Just like the intermittency factor in Fig. 8, the burst rate would remain almost constant inside the boundary layer, but change significantly at the outer edge of the boundary layer, so similarly the ensemble statistics is considered within $y/\delta^* = [0.5,\ 3]$.

In the classical theory of the stochastic concentrated breakdown, the burst rate is found to be proportional to $(1-\gamma)\sqrt{-\ln(1-\gamma)}$ [14,17]. The ensemble statistics of the experimental results of the normalized burst rate $B/B_{\max}$ ($B_{\max}$ is the maximum burst rate in the breakdown region) are shown in Fig. 11, and significant deviation from the classical theory is observed. Specifically, the burst rate obtained from experiments is lower than the prediction of $2.33(1-\gamma)\sqrt{-\ln(1-\gamma)}$ when $\gamma < 0.5$ but becomes larger than the prediction when $\gamma > 0.5$. (The coefficient 2.33 is added to make the peak value of the curve to be 1.) It is noted that the experimental results can be well fitted by a quadratic function $3.8\gamma(1-0.96\gamma)$, and it means that the distribution is quite symmetric. As argued by Vinod and Govindarajan [14,15], the more regular the breakdown pattern is, the more symmetric the burst rate distribution with respect to $\gamma = 0.5$. This situation usually occurs when the transition is dominated by a strong laminar instability mode (e.g., K- or H-type transition). So it is possible that the breakdown is much regular in present step-induced transition although the symmetry axis is slightly different from $\gamma = 0.5$.

The burst rate obtained from the simulation case C-E of the stochastic concentrated breakdown agrees quite well with the classical theory. It means that some hypothesis used in the simulation is no longer true in the step-induced transition process, and being nonstochastic is just one of the possibilities, as well as being nonconcentrated or non-Poisson. To identify the pattern of breakdown, more details of the transition should be examined.

If the breakdown occurs in a regular pattern, the binary sequence of the intermittency function must show some periodicity, which probably can be detected from the power spectrum. As shown in Fig. 12, the power spectrums of $\Gamma(t)$ at $x = 700$, 750, and 800 mm, which corresponds to $\gamma = 0.33$, 0.51, and 0.67, are obtained from the ensemble statistics in a similar way with γ and B. A distinct peak at 2.4 Hz can be observed in the spectrum at all the stations, and no higher harmonics or subharmonics are detected. It indicates that the

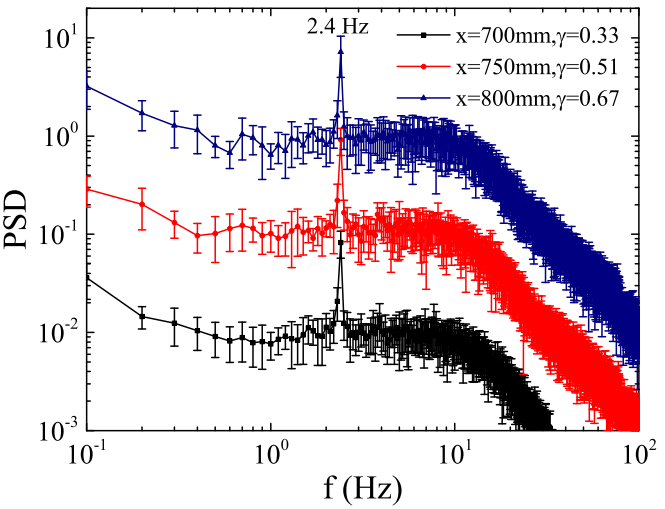

FIG. 12. Power spectrum for the binary sequence of the intermittency function (the data are shifted in the vertical direction for clarity) obtained from experimental data. Error bars indicate standard deviation from the ensemble average.

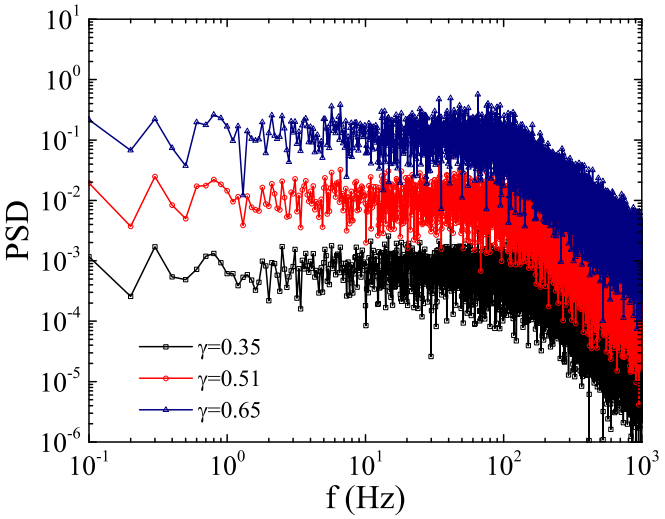

FIG. 13. Power spectrum for the binary sequence of the intermittency function (the data are shifted in the vertical direction for clarity) obtained from cellular-automaton simulation of a stochastic concentrated breakdown process (case C-E).

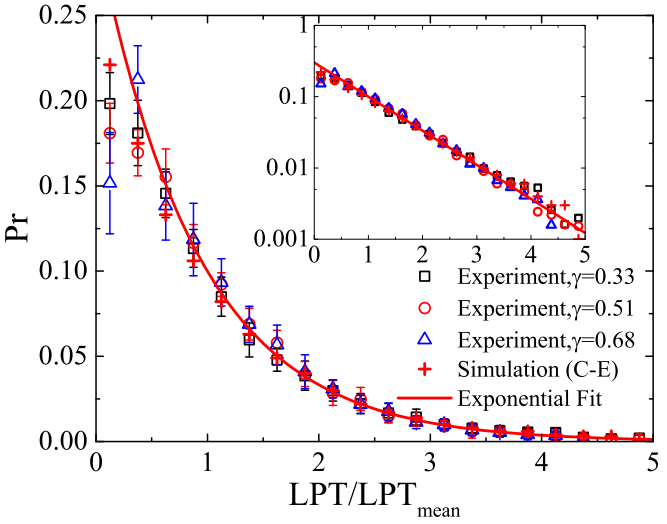

FIG. 14. Probability distribution of the laminar persistence time at three stations $x = 700$, 750, and 800 mm corresponding to $\gamma = 0.33$, 0.51, and 0.68, and the simulation result of case C-E at $\gamma = 0.33$. Error bars indicate standard deviation from the ensemble average. The data are plotted in log-linear coordinates in the inset.

regular pattern might exist, but it is just a small part of the breakdown. This 2.4-Hz low-frequency oscillation is probably related to the 2.3-Hz fluctuation in the free stream because the boundary layer can become unsteady due to the influence of the free stream.

To contrast this periodicity, the power spectrums of the numerical results of case C-E are plotted in Fig. 13. Here, each time step in the simulation is assumed to be the same with the sampling interval. As expected, no peaks in the spectrum can be observed, which is consistent with the setup of the completely stochastic spot generation.

In a real flow, the randomness in the environment can never be eliminated, so the $\Gamma(t)$ time series would always be at least partly stochastic. According to the power spectrum, the proportion of the regular pattern in the step-induced transition can be roughly estimated from the burst number in regular pattern (multiply 2.4 Hz by 60 s which is the length of the time series) divided by the total burst number in $\Gamma(t)$. Then, we can obtain that about 23% of the spots in regular pattern at $x = 700$ mm and, similarly, 21% at $x = 750$ mm and 22% at $x = 800$ mm. The true percentage is even lower considering the possible spot merger. According to the results of Vinod and Govindarajan [14], if the transition process is a combination of concentrated regular and stochastic breakdown, the approximately symmetric distribution of $B/B_{\max}$ can be obtained when the proportion of the regularly generated spots is 90%, and considerable deviation from the symmetric distribution can be found when the percentage is 50%. The present experimental result is probably lower than 50%, although the true percentage of regular pattern is difficult to measure directly since the spanwise distribution of the regular spot generation is unknown. Thus, it would be helpful and necessary to examine the regularity in another way.

As shown by Vinod and Govindarajan [14], the existence of the regular pattern can also be examined from the probability distribution of the laminar persistence time (LPT). The LPT is estimated as persistence time between two subsequent turbulent fragments in the $\Gamma(t)$ time series. If the concentrated breakdown process is completely stochastic, an exponential decay is expected in the distribution of LPT, otherwise large modulations or flat portions can be observed when the regular pattern plays an important role.

The probability distributions of LPT (normalized by the mean value) obtained in the present experiments are shown in Fig. 14. The probability is first counted at each wall-normal location and then averaged within $y/\delta^* = [0.5, 3.0]$. Similar results are obtained at different stages of the breakdown. Generally, exponential decay is observed in the most part of the probability distributions, as shown in the insets with log-linear coordinates. The slight deviation from the exponential decay might be attributed to the small amount of regularly generated spots or the mild imperfection of the laminar-turbulent separation technique. No distinct flat portion or large modulations can be observed in the experimental results. It indicates that the breakdown is mostly a stochastic process, rather than dominated by the regular pattern. Since only existence of the regular pattern would result in the significant variation of the statistics in the spanwise direction (e.g., the K- or H-type transition), the exponential decay of the probability distribution of LPT also indicates that there would be no significant variation in the spanwise direction of the breakdown region in a statistical sense.

Since the deviation of the experimental results from the classical theory cannot be attributed to the regular pattern, it is necessary to search for other possible explanations based on stochastic spot generation process.

The probability distribution of LPT obtained from the simulation case C-E at $\gamma = 0.33$ is also plotted in Fig. 14 for comparison, and exponential decay is observed as expected by the classical theory. Together with the above results of γ

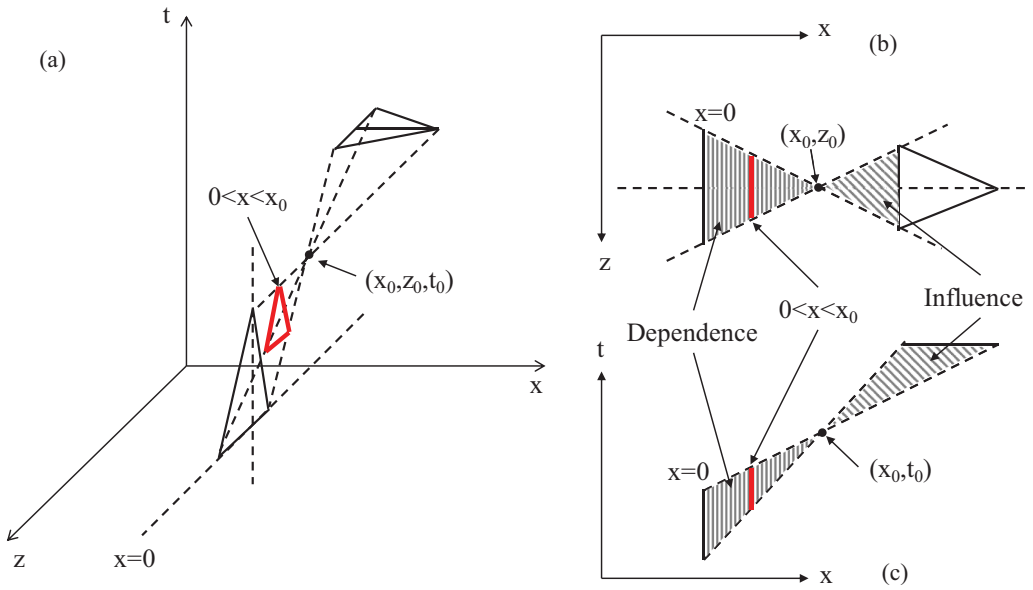

FIG. 15. Sketch of the heuristic analysis of the breakdown process. (a) The three-dimensional region projected by the two-dimensional breakdown region considering time (t) as the vertical axis. As time goes on, the downstream evolution and propagation of the triangular turbulent spot generated at (x_0, z_0, t_0) forms the three-dimensional influence region. Similarly, any turbulent flow in the upstream dependence region would pass the point (x_0, z_0, t_0). The red triangle is a cross section at some streamwise location $(0 < x < x_0)$ upstream of (x_0, z_0, t_0). (b), (c) Top and side views of (a), and the straight boundary lines correspond to the linear propagation of the turbulent spots.

and B, the simulation of the concentrated Poisson stochastic breakdown can accurately reproduce the predictions of the classical theory of the breakdown process, which verifies the simulation to be a reliable tool in the following discussion.

VI. HEURISTIC ANALYSIS

In this section, a heuristic analysis of the transition process is presented from a probabilistic view following the idea of Emmons [4]. The turbulent spot is assumed to be triangular, which is consistent with the cellular-automaton simulation. The propagation of the turbulent spot is considered in a three-dimensional coordinate system, as shown in Fig. 15, where the axes in the horizontal plane represent the streamwise and spanwise positions in the transition zone and the vertical axis represent the time. As time goes on, the turbulent spot generated at the point (x_0, z_0, t_0) would propagate downstream and expand in both the streamwise direction and two lateral sides, which forms a three-dimensional region influenced by (x_0, z_0, t_0). It means that if the flow at (x_0, z_0, t_0) is turbulent, the influence region would all be turbulent. Similarly, there is a dependence region of (x_0, z_0, t_0) at upstream locations. If there exists a turbulent spot anywhere in the dependence region, the flow at (x_0, z_0, t_0) would be turbulent. The probability of (x_0, z_0, t_0) to be turbulent (the intermittency factor γ) can be estimated by the following procedure.

For the location x ($0 < x < x_0$, and $x = 0$ represents the leading edge of the plate), assume $G(x)$ is the probability that there is turbulence in the dependence region upstream of x, so that $G(0) = 0$ and $G(x_0) = \gamma(x_0)$. Then, the probability that there is turbulence in the vertical cross section at $0 < x < x_0$ is $\partial G(x)/\partial x$, as marked by the red triangular region in Fig. 15. On the other hand, we assume that this probability can be described by a local integration $[1 - G(x)] \int_S g(x) dz\, dt$, where S is the measure of the triangular area in the cross section, and $g(x)$ is the average spot generation rate per unit time and per unit streamwise and spanwise space, which is independent of z and t. $[1 - G(x)]$ is multiplied to ensure that no spots are generated before x in the dependence region, and to avoid that one spot is counted more than once. So, we have an equation

$$\frac{\partial G(x)}{\partial x} = [1 - G(x)] \int_S g\, dz\, dt \tag{21}$$

which is equal to

$$\frac{\partial \ln[1 - G(x)]}{\partial x} = -\int_S g\, dz\, dt. \tag{22}$$

Since $G(0) = 0$, we can integrate the above equation on both sides from $x = 0$ to $x = x_0$ and obtain the following equation:

$$\ln[1 - G(x_0)] = -\int_V g\, dx\, dz\, dt, \tag{23}$$

where V is the entire three-dimensional dependence region of $p(x_0, z_0, t_0)$. Since $G(x_0) = \gamma(x_0)$,

$$\gamma(x_0) = 1 - \exp\left(-\int_V g\, dx\, dz\, dt\right). \tag{24}$$

Since it is an integration on a three-dimensional space-time domain, Emmons [4] argued that $\int_V g\, dx\, dz\, dt \propto x_0^3$, and obtained

$$\gamma(x_0) = 1 - \exp\left(-A_{03} x_0^3\right), \tag{25}$$

where A_{03} is a parameter depending on the spot generation rate.

Later, the concentrated breakdown hypothesis is proposed and it is argued that $\int_V g\, dx\, dz\, dt \propto x_0^2$ by assuming $g(x)$ is a

Dirac delta function,

$$g = \begin{cases} g_c, & x = x_s \\ 0, & x \neq x_s \end{cases} \tag{26}$$

where g_c is the average spot generation rate per unit time and per unit spanwise distance concentrated at x_s [16]. So that

$$\gamma(x_0) = 1 - \exp\left(-A_{02}x_0^2\right), \tag{27}$$

where A_{02} is a coefficient proportional to g_c. Note that Eq. (27) is equivalent to Eq. (16) of classical theory. This intermittency growth curve is assumed to be correct for a flat-plate boundary-layer flow. For instance, in the axial symmetrical conical flow, it was derived by Cebeci and Smith [35] that the intermittency curve is as

$$\gamma(x_0) = 1 - \exp\left[-A_{\text{cone}} \ln \frac{x_0}{x_s}(x_0 - x_s)\right], \tag{28}$$

where A_{cone} is the spot propagation parameter, x_s is the location of the start of the transition [21].

Even for the flat-plate boundary-layer flow, it is found that the distribution given by Eq. (27) is not always that accurate. For instance, Johnson and Fashifar [17] noticed that Eq. (25) is better to fit their experimental data than Eq. (27). Recently, Kreilos *et al.* [18] also reported that Eq. (27) cannot accurately reproduce the intermittency distributions in their simulation results of the bypass transition under various high free-stream turbulence level.

Without losing generality, for present flat-plate boundary layer we assume that there is a starting location x_s ($0 < x_s < x_0$) where no spots are generated upstream of x_s, and there exists the spot generation rate g which satisfies the following relation:

$$\int_V g\,dx\,dz\,dt \propto (x_0 - x_s)^n. \tag{29}$$

So, the intermittency distribution can be transformed into the form

$$\gamma(x_0) = 1 - \exp(-A_n\xi^n) \tag{30}$$

by introducing the normalized streamwise location ξ [defined by Eq. (17)] and

$$A_n = \{[-\ln(1-0.75)]^{\frac{1}{n}} - [-\ln(1-0.25)]^{\frac{1}{n}}\}^n. \tag{31}$$

This equation can be derived based on the definition of $x_{0.25}$ and $x_{0.75}$. Specifically, $A_2 = 0.41095$, $A_3 = 0.09412$, $A_4 = 0.01548$, and $A_{4.62} = 0.00463$.

As for the parameter F, if we continue to use the definition $F = \sqrt{-\ln(1-\gamma)}$, then

$$F = (A_n\xi^n)^{1/2}. \tag{32}$$

So, F would be a linear function of ξ only when $n = 2$, which recovers the result in the classical theory.

Since the spot propagation parameter is almost unchanged in the breakdown process [14,16,22], the growth of the intermittency factor can be taken as the overall effect of the growth of each individual spot, hence the following relation can be obtained:

$$d\gamma/dx \propto B, \tag{33}$$

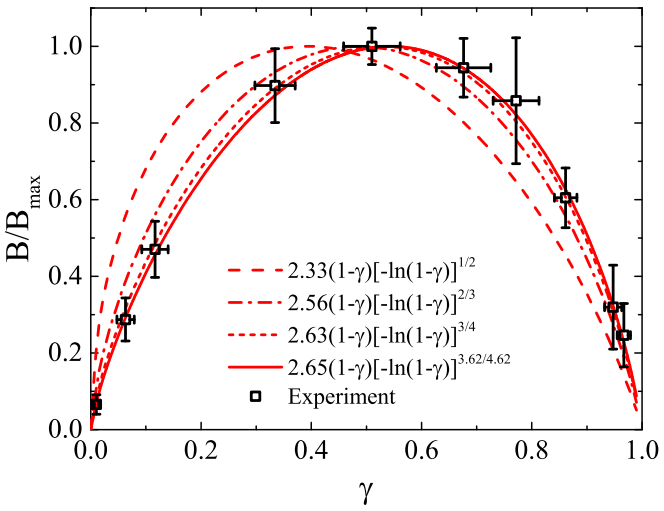

FIG. 16. Experimental results of the burst rate (black squares) in comparison with the distribution in various breakdown scenarios predicted by the heuristic analysis (normalized by the maximum burst rate) $B \propto [-\ln(1-\gamma)]^{\frac{n-1}{n}}(1-\gamma)$ with various n (red lines).

and further we can obtain

$$B \propto [-\ln(1-\gamma)]^{\frac{n-1}{n}}(1-\gamma). \tag{34}$$

Obviously, the distribution of the burst rate depends on $g(x)$ and n.

As shown in Fig. 16, the experimental results can be well fitted using Eq. (34) with $n = 4.62$. As n increases from 2 to 4.62, the maximum value of the normalized burst rate would be obtained at larger γ, and as a result, the distribution of the burst rate becomes more and more symmetric. The growth curve of the intermittency factor with various n are plotted versus x instead of ξ to compare with the experimental results, as shown in Fig. 17. Since the transition starting location (x_s)

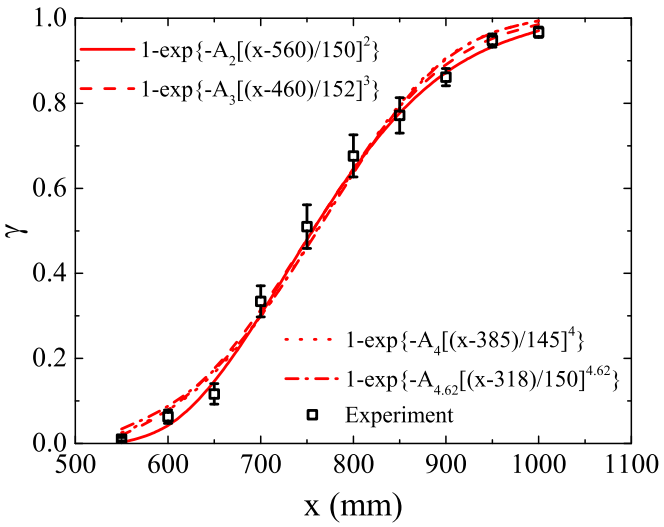

FIG. 17. Experimental results of the intermittency factor (black squares) fitted with the distribution in various breakdown scenarios predicted by the heuristic analysis: $\gamma = 1 - \exp\{-A_n[(x-x_s)/(x_{0.75}-x_{0.25})]^n\}$ with various n (red lines).

and the length scale of the transition region $(x_{0.75} - x_{0.25})$ are unknown, they are adjusted to achieve the best fitting result. All the curves are very close and acceptable to fit the experimental data. It indicates that the distribution of the intermittency factor is not as sensitive as the burst rate to the parameter n.

The pattern of breakdown can be interpreted from the fitting results as follows. Rewrite the left side of Eq. (29) as

$$\int_V g\,dx\,dz\,dt = \int_{x_s}^{x_0} g(x)S(x)dx. \tag{35}$$

Assume that $g(x) \propto (x - x_s)^m$, and considering that $S(x) \propto (x - x_s)^2$, then $\int_V g\,dx\,dy\,dt \propto (x_0 - x_s)^{m+3}$, hence, $n = m + 3$. So with $n = 4.62$, we have $g(x) \propto (x - x_s)^{1.62}$. The average interarrival time in spot generation would decrease as $1/(x - x_s)^{1.62}$ throughout the breakdown region. Thus, the present step-induced transition is identified to be not concentrated, but a distributed breakdown. The pattern of distributed breakdown probably indicates that this is a bypass transition, which is different from the understanding in existing studies about the step-induced transition. The reason is as follows.

According to previous studies on the mechanism of the bypass transition [36], the turbulent spots would be generated due to the secondary instability of the boundary-layer streaks [37]. Due to the free-stream low-frequency fluctuations, the streaks are generated by boundary-layer disturbances in the form of streamwise vortices via the lift-up effect [38]. The high-frequency fluctuations cannot penetrate deep enough to perturb the flow inside the boundary layer due to the shear-sheltering effect [39,40], but the interaction of the high-frequency fluctuation with the streaks at the outer edge of the boundary layer can trigger the secondary instability and lead to the generation of turbulent spots [41,42].

Since the streak breakdown is random in both time and space [43], the spot generation in a bypass transition is not concentrated but distributed. The possibly existing regular pattern might be related to a discrete instability mode generated in the flow around the step, and the interaction of the discrete and continuous modes could also trigger the bypass transition even if neither mode alone is sufficiently strong [44,45]. Another possible reason for the bypass transition could be that the boundary-layer receptivity to the free-stream disturbances is enhanced by the step. Note that the free-stream turbulence level in the present experimental setup is not high enough to induce a typical bypass transition in the flat-plate boundary layer. As mentioned by Rizzetta and Visbal [5], the step might have two effects on the boundary layer, one is to enhance the receptivity and the other is to generate discrete instability modes. Most existing research is focusing on the latter, but the results in this paper provide experimental evidences that the former one might also be important.

Previous studies also can provide the evidence that the distributed breakdown is related to the bypass transition. For instance, Kreilos *et al.* [18] found that the growth curves of the intermittency factor in bypass transition (Tu = 3%–4%) cannot be reproduced by the classical theory with concentrated breakdown hypothesis. Another example can be found in the experimental results of Johnson and Fashifar [17], and they proposed a new model which turns out to be a pattern of distributed breakdown discussed above.

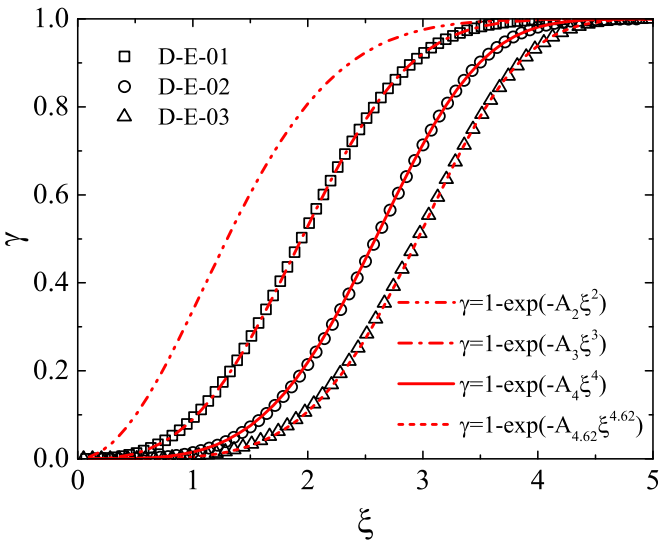

FIG. 18. Comparison of the growth curves of the intermittency factor (γ) predicted by the heuristic analysis [red lines, $\gamma = 1 - \exp(-A_n\xi^n)$, $n = 3, 4, 4.62$] and the statistical results of the numerical simulations of the distributed breakdown (open symbols: D-E-01 square, D-E-02 circle, D-E-03 triangular). The distribution of γ in classical theory [$\gamma = 1 - \exp(-A_2\xi^2)$, dashed-dotted-dotted line] is also plotted as a reference.

VII. SIMULATION RESULTS

In this section, we present the numerical simulation results to validate the heuristic analysis. In cases D-E-01, D-E-02, and D-E-03, the distribution of the average spot generation rate is set according to the observation of $g(x) \propto (x - x_s)^m$, where $m = 0$, 1, and 1.62. The spot generation is assumed to be an independent Poisson process at every streamwise grid location. The average interarrival time (β) is inversely proportional to the average spot generation rate, and the distribution of β is chosen based on numerical tests to find a proper length of the breakdown region. If the above analysis is correct, the simulation results of D-E-01, D-E-02, and D-E-03 should be consistent with the predictions of Eqs. (30), (32), and (34), in which $n = 3$, 4, and 4.62.

The growth curves of the intermittency factor obtained from the statistical results of the distributed breakdown simulations are shown in Fig. 18. Excellent agreement with the predictions of the heuristic analysis is observed. As n increases, the deviation of the γ distribution from the prediction of the classical theory is more and more significant. When n is large, the growth of γ is greatly suppressed before ξ increases to 1, and it takes a longer distance for γ to reach 0.1. This result is reasonable since the spot generation rate would be very low in the early stage of breakdown for the cases with large n. Approaching to the end of the breakdown, the growth of γ is affected by the merger of turbulent spots, which causes the slowdown of the growth of γ. In the distributed breakdown,

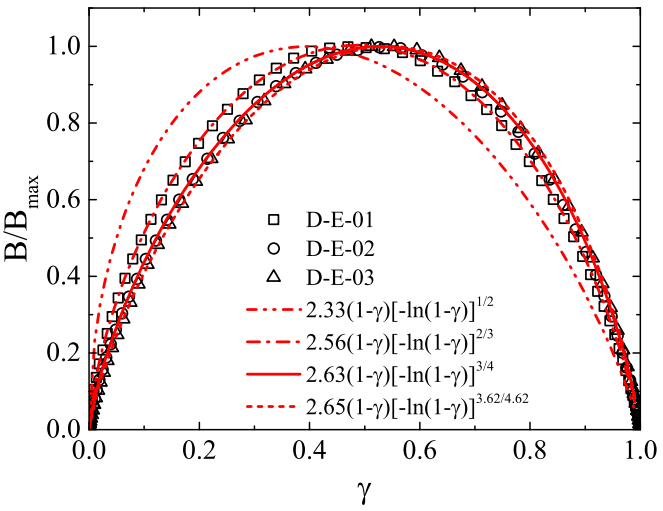

FIG. 19. Comparison of the distributions of the normalized burst rate ($B/B_{\max}$) predicted by the heuristic analysis (red lines, $B \propto (1-\gamma)[-\ln(1-\gamma)]^{(n-1)/n}$, $n = 3,\ 4,\ 4.62$) and the statistical results of the numerical simulations of the distributed breakdown (open symbols: D-E-01 square, D-E-02 circle, D-E-03 triangular). The distribution of $B/B_{\max}$ in classical theory ($B/B_{\max} = 2.33(1-\gamma)[-\ln(1-\gamma)]^{1/2}$, dashed-dotted-dotted line) is also plotted as a reference.

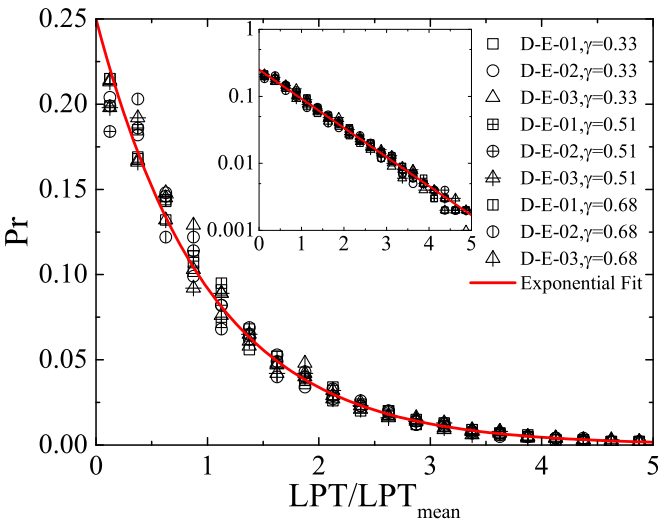

FIG. 20. Statistical results of the probability distribution of the normalized laminar persistence time ($\mathrm{LPT}/\mathrm{LPT}_{\mathrm{mean}}$) at different stages of breakdown ($\gamma = 0.33,\ 0.51,\ 0.68$) in the distributed stochastic breakdown simulations (D-E-01, D-E-02, D-E-03). An exponential distribution fitted from the simulation results is also plotted as a reference (red line). The results are plotted in log-linear coordinates in the inset.

this situation is changed due to the newly generated turbulent spot, and that makes γ approach to 1 more quickly.

The burst rate distributions of the distributed breakdown process obtained from the statistics of the numerical simulation results and the heuristic analysis are shown in Fig. 19, and excellent agreement is obtained again. Although we have the relation $d\gamma/dx \propto B$, the derivative of γ cannot be directly estimated especially from experimental results since the spacing of the measurement stations is too large. The statistical distribution of the burst rate as a function of γ is more reliable to identify the pattern of breakdown than the growth curve of γ as a function of ξ since the calculation of ξ would be inevitably arbitrary.

All the predictions (γ, F, B) of our heuristic analysis have been validated by the statistical results of the numerical simulations, and these results are helpful to confirm the pattern of breakdown identified in the previous section. In addition, the probability distributions of the laminar persistence time (LPT) for distributed breakdown are also examined from the simulation results. As shown in Fig. 20, exponential decay of the distributions is observed all three cases at different stages of breakdown ($\gamma = 0.33,\ 0.51,\ 0.68$), and this is consistent with the experimental results shown in Fig. 14. It indicates that the probability distribution of LPT cannot be used to distinguish the concentrated and distributed breakdown.

VIII. DISCUSSION

Since the pattern of breakdown depends on the generation of turbulent spots, the effects of the spatial and temporal characteristics of the spot generation on the breakdown statistics are further discussed in this section.

A. Quasiconcentrated breakdown

The concentrated and distributed breakdown are different in the streamwise region of spot generation. In a real transition process, the generation of turbulent spots cannot be concentrated precisely at the same streamwise location. In the following discussion, the breakdown will be referred as quasiconcentrated (QC for short) if the spots are generated in a single Poisson process and in a streamwise region of finite size. Will the statistics of the quasiconcentrated breakdown become close to a distributed breakdown? To answer this question, further simulations are performed and the parameters are shown in Table II. The average spot generation rate is the same in these cases, but the streamwise length of the spot generation region is gradually increased from case QC-E-01 to case QC-E-04. Specifically, the spot generation region is as long as half of the whole simulation region in case QC-E-04.

The statistical results of the intermittency factor are shown in Fig. 21 in comparison with the prediction of the classical theory. Generally, the growth curves of γ are coincident with the classical theory [$\gamma = 1 - \exp(-A_2\xi^2)$] except for some slight deviation at $\xi < 0.5$. It means that the quasiconcentrated breakdown is significantly different from the distributed breakdown. Note that the nominal starting location of breakdown (x_s) is set to be negative to obtain the best fitting result. It is shown more clearly in the inset figure that the deviation is reduced as the streamwise length of the spot generation region decreases, and it indicates that the concentrated breakdown hypothesis in the classical theory would be a good approximation. Similar conclusion can be obtained from the results of the parameter F and the burst rate, and those results are not shown for simplicity.

TABLE II. Setup and parameters for the simulations of quasiconcentrated and non-Poisson-process breakdown.

Simulation case	Interarrival time distribution	Parameter	Streamwise region of spot generation (X)	Type of breakdown
QC-E-01	Exponential	β=15	[1,10]	Quasiconcentrated
QC-E-02	Exponential	β=15	[1,20]	Quasiconcentrated
QC-E-03	Exponential	β=15	[1,50]	Quasiconcentrated
QC-E-04	Exponential	β=15	[1,100]	Quasiconcentrated
C-G	Gaussian	$\mu = \sigma^2 = 15$	1	Concentrated
D-G	Gaussian	$\mu = \sigma^2 = 300000/X^{1.62}$	[1,200]	Distributed

B. Beyond Poisson process

In a previous discussion it is assumed that the spot generation is a Poisson process. However, this hypothesis has not been used explicitly in the heuristic analysis. Will the spot generation of non-Poisson process lead to a much different statistical result? To answer this question, another two simulations of the concentrated and distributed breakdown (C-G and D-G) are performed. In these two cases, the interarrival time of spot generation is set to have a Gaussian probability distribution, and the setup and parameters can be found in Table II. Specifically, in cases C-G and D-G, the spot generation rate is set to be the same with that in cases C-E and D-E-03, respectively, so the predictions of the classical theory and the heuristic analysis are expected if the non-Poisson process has no influence.

The statistical results obtained from the non-Poisson-process simulations are shown in Fig. 22. The results of the concentrated breakdown (C-G) deviate a lot from the classical theory, and this deviation should be attributed to the different scenarios in spot merger. As shown in Fig. 5, the probability of the exponential distribution for Poisson process is larger than that of the Gaussian distribution for very small and very large interarrival time. It means that the spots generated from Poisson process would be more probable to be very close to each other, as well as very far from each other. If the spots are very close in space, spot merger would be easy in the early stage of breakdown, and the intermittency factor would correspond to a larger burst number. If the spots are very distant in space, spot merger would be difficult even in the late stage of breakdown, and the intermittency factor would correspond to a smaller burst number. This is consistent with the observation that the burst rate prediction of classical theory (Poisson process) is larger than the C-G simulation at $\xi < 0.4$, but smaller at $\xi > 0.4$, as shown in Fig. 22.

It is also interesting to observe that the burst rate distribution of the distributed breakdown (D-G) agrees quite well with the heuristic analysis prediction. It indicates the spot merger is mostly affected by the newly generated spots. More importantly for the experimental results, the transition is identified to be a distributed breakdown no matter if the spot generation is a Poisson process or not.

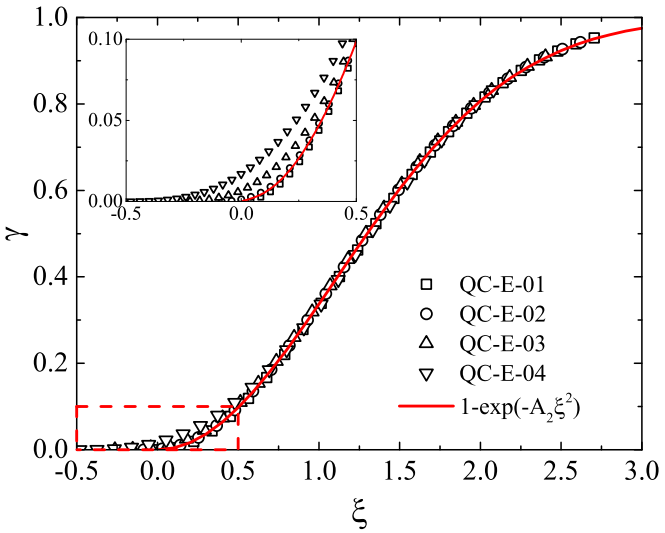

FIG. 21. The statistical results of the intermittency factor (γ, open symbols) as a function of ξ obtained from the quasiconcentrated breakdown simulations (QC-E-01, QC-E-02, QC-E-03, QC-E-04). The prediction of the classical theory (red line) is also plotted for comparison. The region in the lower left corner is plotted in the inset for clarity.

IX. SUMMARY AND CONCLUSION

In this paper, the pattern of breakdown in the step-induced transition is investigated based on binary sequence statistics and the cellular-automaton simulations. The main findings are as follows.

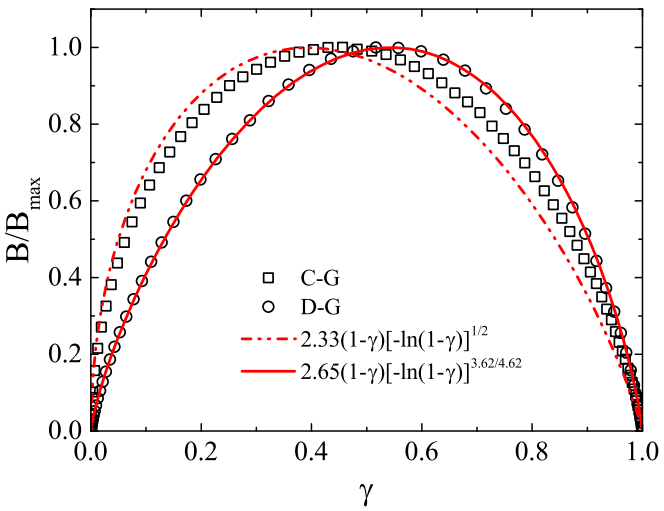

FIG. 22. Statistical results of the normalized burst rate ($B/B_{\max}$) obtained in the simulation of non-Poisson process of concentrated (squares) and distributed (circles) breakdown. The predictions of the classical theory (dashed-dotted-dotted line) and the heuristic analysis (solid line) are also plotted for comparison.

First, it is found that the statistics of the burst rate significantly deviate from the classical theory of concentrated breakdown hypothesis. It is also shown that this deviation cannot be attributed to the regular pattern of spot generation based on the analysis of power spectrum and laminar persistence time.

Second, a heuristic analysis of the breakdown process is performed from a probabilistic view, and it identifies that the present step-induced transition has a pattern of distributed breakdown. This pattern is probably related to the bypass transition, which is different from the current understanding about the step-induced transition. The possible reason for the bypass transition is attributed to the discrete and continuous modes interaction, or the boundary-layer receptivity to the free-stream turbulence enhanced by the step. The heuristic analysis is validated by the cellular-automaton simulations.

Third, the effects of the quasiconcentration and non-Poisson process in spot generation on the breakdown statistics are studied based on the simulation results. It is found that the statistical results of the quasiconcentrated breakdown can be well predicted by the classical theory. It indicates that the pattern of distributed breakdown proposed in this paper is fundamentally different from the concentrated breakdown scenarios not only just in the location of spot generation. Specifically, in a distributed breakdown, multiple turbulent spots can be independently and simultaneously at various streamwise locations of the breakdown region, while only a single one spot generation sequence is considered in the classical theory of concentrated breakdown. It is also shown that the results of the non-Poisson process in spot generation can be accurately reproduced by the heuristic analysis. It indicates that the non-Poisson process of spot generation would not hamper the identification of the distributed breakdown.

ACKNOWLEDGMENTS

This work was supported by the National Natural Science Foundation of China (Grants No. 11772033 and No. 91752201) and the China-European Union Aeronautical Science and Technology Cooperation Project DRAGY. We acknowledge computing support provided by Center for Computational Science and Engineering of Southern University of Science and Technology.

[1] W. S. Saric, H. L. Reed, and E. J. Kerschen, Annu. Rev. Fluid Mech. **34**, 291 (2002).
[2] Y. S. Kachanov, Annu. Rev. Fluid Mech. **26**, 411 (1994).
[3] L. N. Trefethen, A. E. Trefethen, S. C. Reddy, and T. A. Driscoll, Science **261**, 578 (1993).
[4] H. Emmons, J. Aeronaut. Sci. **18**, 490 (1951).
[5] D. P. Rizzetta and M. R. Visbal, AIAA J. **52**, 385 (2014).
[6] C. A. Edelmann and U. Rist, AIAA J. **53**, 2504 (2015).
[7] A. Inasawa, J. M. Floryan, and M. Asai, Theor. Comput. Fluid Dyn. **28**, 427 (2014).
[8] W. Zhang, P. Liu, and H. Guo, AIAA J. **56**, 2471 (2018).
[9] Y. X. Wang and M. Gaster, Exp. Fluids **39**, 679 (2005).
[10] A. Worner, U. Rist, and S. Wagner, AIAA J. **41**, 192 (2003).
[11] X. S. Wu and L. W. Hogg, J. Fluid Mech. **550**, 307 (2006).
[12] H. Xu, S. Sherwin, P. Hall, and X. S. Wu, J. Fluid Mech. **792**, 499 (2016).
[13] H. Xu, J.-E. W. Lombard, and S. J. Sherwin, J. Fluid Mech. **817**, 138 (2017).
[14] N. Vinod and R. Govindarajan, Phys. Rev. Lett. **93**, 114501 (2004).
[15] N. Vinod and R. Govindarajan, J. Turbul. **8**, N2 (2007).
[16] R. Narasimha, Prog. Aerosp. Sci. **22**, 29 (1985).
[17] M. W. Johnson and A. Fashifar, Int. J. Heat Fluid Flow **20**, 95 (1994).
[18] T. Kreilos, T. Khapko, P. Schlatter, Y. Duguet, D. S. Henningson, and B. Eckhardt, Phys. Rev. Fluids **1**, 043602 (2016).
[19] D. Barkley, Phys. Rev. E **84**, 016309 (2011).
[20] K. T. Allhoff and B. Eckhardt, Fluid Dyn. Res. **44**, 031201 (2012).
[21] J. S. Jewell, I. A. Leyva, and J. E. Shepherd, Exp. Fluids **58**, 32 (2017).
[22] J. H. M. Fransson, Phys. Rev. E **81**, 035301(R) (2010)
[23] I. Wygnanski, in *The Role of Coherent Structures in Modelling Turbulence and Mixing*, edited by J. Jimenez, Lecture Notes in Physics (Springer, Berlin, 1981), Vol. 136.
[24] P. S. Klebanoff, K. D. Tidstrom, and L. M. Sargent, J. Fluid Mech. **12**, 1 (1962).
[25] Y. S. Kachanov, V. V. Kozlov, and V. Y. Levchenko, Fluid Dyn. **12**, 383 (1977).
[26] Y. S. Kachanov and V. Y. Levchenko, J. Fluid Mech. **138**, 209 (1984).
[27] P. Liu, Y. Xing, H. Guo, and L. Li, Appl. Acoust. **116**, 65 (2017).
[28] B. Cantwell, D. Coles, and P. Dimotakis, J. Fluid Mech. **87**, 641 (1978).
[29] S. K. Robinson, Annu. Rev. Fluid Mech. **23**, 601 (1991).
[30] R. A. Antonia, Annu. Rev. Fluid Mech. **13**, 131 (1981).
[31] T. Hedley and J. Keffer, J. Fluid Mech. **64**, 625 (1974).
[32] R. J. Volino, M. P. Schultz, and C. M. Pratt, ASME J. Fluids Eng. **125**, 28 (2003).
[33] J. Wang, M. Wan, S. Chen, and S. Chen., J. Fluid Mech. **841**, 581 (2018).
[34] T. Sayadi, C. W. Hamman, and P. Moin, J. Fluid Mech. **724**, 480 (2013).
[35] T. Cebeci and A. M. O. Smith, *Analysis of Turbulent Boundary Layers* (Academic, London, 1974).
[36] P. Durbin and X. Wu, Annu. Rev. Fluid Mech. **39**, 107 (2007).
[37] M. Asai, M. Minagawa, and M. Nishioka, J. Fluid Mech. **455**, 289 (2002).
[38] P. J. Schmid and D. S. Henningson, *Stability and Transition in Shear Flows* (Springer, New York, 2001).
[39] R. G. Jacobs and P. A. Durbin, Phys. Fluids **10**, 2006 (1998).
[40] R. G. Jacobs and P. A. Durbin, J. Fluid Mech. **428**, 185 (2000).
[41] T. A. Zaki and P. A. Durbin, J. Fluid Mech. **531**, 85 (2005).
[42] T. A. Zaki and P. A. Durbin, J. Fluid Mech. **563**, 357 (2006).
[43] L. Brandt and H. C. de Lange, Phys. Fluids **20**, 024107 (2008).
[44] Y. Liu, T. A. Zaki, and P. A. Durbin, J. Fluid Mech. **604**, 199 (2008).
[45] R. Bose and P. A. Durbin, Phys. Fluids **28**, 114105 (2016).